Target normal sheath ion acceleration by fs laser irradiating metal/reduced graphene oxide targets

L. Torrisi,[a,d,1] **M. Rosinski,**[b] **M. Cutroneo,**[c] **A. Torrisi,**[d] **J. Badziak,**[b] **A. Zaras-Szydlowska**[b] **and P. Parys**[b]

[a]*Dipartimento di Scienze Fisiche-MIFT, Università di Messina,*
  S. Agata, Italy

[b]*Institute of Plasma Physics and Laser Microfusion,*
  Warsaw, Poland

[c]*Nuclear Physics Institute, AS CR,*
  Rez, Czech Republic

[d]*Istituto Nazionale di Fisica, Sezione di Catania,*
  Catania, Italy

  E-mail: lorenzo.torrisi@unime.it

ABSTRACT: Target normal sheath ion acceleration is applied with a high contrast *fs* laser irradiating advanced targets based on thin metallic films (Al, Cu, Ag and Au) covering micrometric foils of reduced graphene oxide (rGO). The laser intensity is of about 10^{18} W/cm^2 and the laser focal position with respect to the target surface is optimized to have the maximum proton acceleration. Plasma diagnostics are investigated using time-of-flight technique employing SiC detectors, ion collectors, and gaf-chromic films. Micrometric aluminum absorbers were employed to separate the faster proton detection by other accelerated ions. At the optimized laser focal position, the maximum proton acceleration of 2.5 MeV and 3.0 MeV energy was obtained using Ag(200 nm) and Au(200 nm) covering rGO(7 μm) targets, respectively. The high proton energy is due to the high electrical and thermal conductivity and high mechanical resistance of the used rGO foils and to the high plasma electron density of the target.

---

[1]Corresponding author.

Contents

1 Introduction

A new technique of ion acceleration consists in the use of high intensity pulsed lasers irradiating thin targets in high vacuum and in the development of a non-equilibrium plasma in which can be generated instantaneous high electric fields driving the ion acceleration in forward direction.

The laser beam interacting with the solid target produces plasma in which electrons are partly separated from ions by the action of the laser field. Between the layer of electrons and the ions, a very strong electric field, up to tens or even hundreds GeV/cm, is produced. This field pulls the ions, which follow the moving electron layer and, as a result, the ions can be accelerated to high energies, which can be higher than 10 MeV/ nucleon [1].

The developed electric fields are a result of the inhomogeneous distribution of density and velocity of plasma electrons and of hydrodynamic thermal pressure.

A well reproducible system of ion acceleration is the so-called target-normal-sheath-acceleration (TNSA) regime employed to accelerate forward direction ions. A few hundred picosecond laser intensities above 10^{16} W/cm^2 can be used to accelerate light and heavy ions [2], while tens fs lasers at 10^{19} W/cm^2 or higher can be used to accelerate light ions [3].

Improvements in the TNSA ion source are suggesting to use special engineering targets to enhance the ion energy, focusing, yield, energy and angular distributions [4, 5]. The laser properties, the irradiation conditions and the target properties can be chosen to improve the ion acceleration process [6, 7]. Nanostructured targets, or multilayers, or containing nanoparticles, or enriched by gold, using foams, special surface roughness and having special geometries, are studied to enhance the process of laser driving ion acceleration [8–10].

This paper investigates the use of targets using micrometric platelet of reduced graphene oxide (rGO), which foil is covered by different metallic films, in order to study their influence on the TNSA forward ion acceleration.

2 Experimental section

The presented experiments were conducted at IPPLM fs laser in Warsaw. A Ti sapphire laser operating at 810 nm wavelength, with a maximum pulse energy of 700 mJ, the main pulse duration

of 45 fs, and a high amplified spontaneous emission contrast of about 10^{-8}, with p-polarized radiation. The laser beam can be focused on the target surface at 9 microns spot diameter.

In our experiment the laser pulse energy was of about 350 mJ, the minimum spot diameter was 9 microns and the maximum laser intensity was 1.2×10^{19} W/cm^2.

The laser hits a solid target constituted by a foil with micrometric thickness placed on a 1 mm diameter hole of a 1 mm thick Al holder having a conical hole with external aperture, as depicted in figure 1a. Figure 1b shows a photo of the target Au (200 nm) / rGO (7 μm). Figure 1c shows a photo of the entire target holder, 2 cm × 3 cm wide, containing 40 holes to attach 40 target foils. Figure 1d reports the intern of the scattering chamber where are positioned the target holder, the focusing parabolic mirror and the ion detectors. Figure 1e shows the external spherical high vacuum chamber with the long pipes used for time-of-flight (TOF) ion detector measurements.
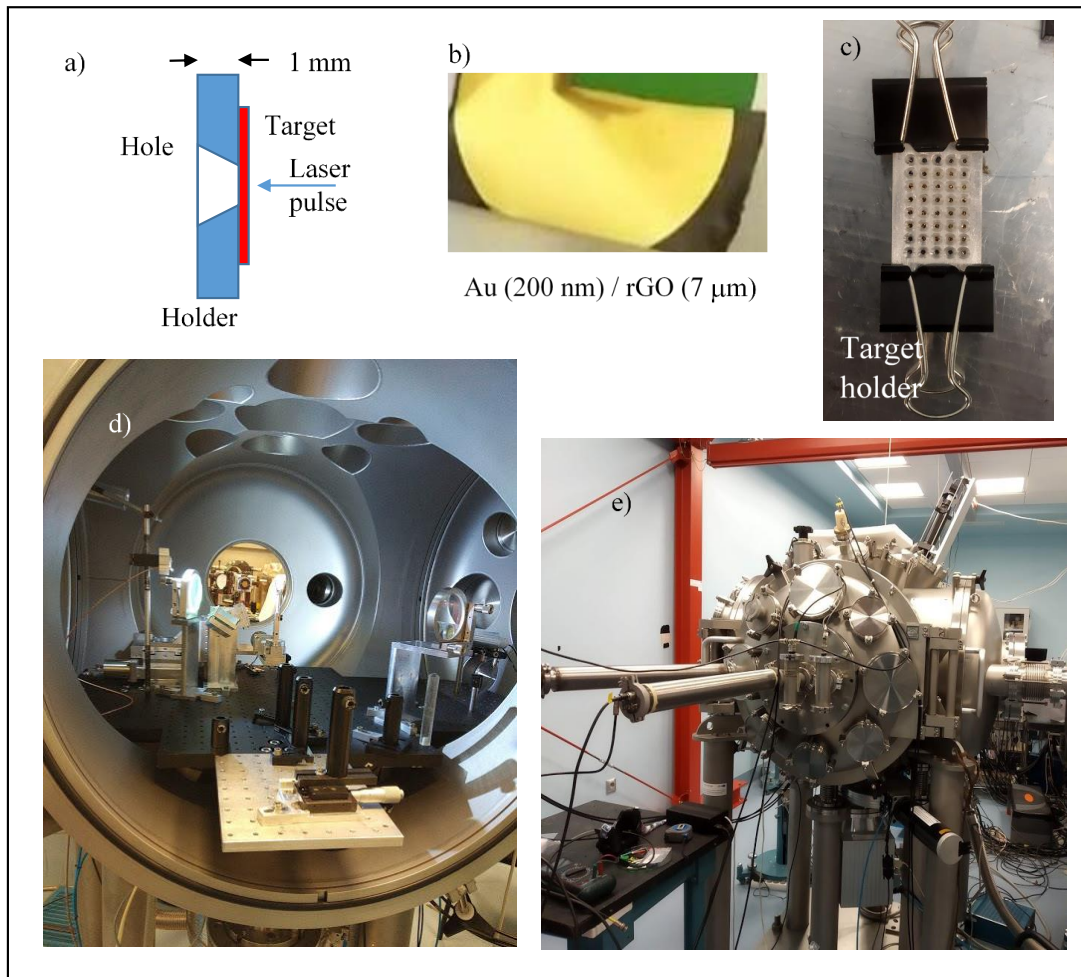

Figure 1. Scheme of the target on the holder hole (a); photo of the target Au (200 nm) / rGO (7 μm) (b); entire target holder (c); intern of the scattering chamber (d); external of the scattering chamber (e).

The target holder is moved in X-Y-Z directions and in angle by micrometric step motors to change the laser spot position on the target, the focal positioning and the incidence angle. The vacuum chamber used for the laser-matter interaction works at a vacuum of 10^{-6} mbar pressure.

Table 1. Composition and some properties of GO and rGO foils.

Material	C (wt%)	H (wt%)	N (wt%)	S (wt%)	O (wt%)	C/O	ρ (g/cm^3)	σ (Ω cm)$^{-1}$	k (W/mK)
GO	46	21	0.5	0.5	32	1.43	1.5	10^{-8}	30
rGO	66.8	15	0.1	0.1	18	3.71	1.9	1.0	2000

The target consists in a foil of reduced graphene oxide (rGO) prepared by using the Graphenea [11] graphene oxide water dispersion (0.4 wt% concentration) according to the technique presented in the literature [12], permitting realizing uniform 7 microns thickness rGO foil. The target foil contains micrometric ($\sim$ 10 microns) platelets, which surface is parallel to the foil surface. The GO reduction occurred thermally during the preparation of the dry foil at 100°C for 3 hours. The physical properties of the foil are typical of the rGO, having high electrical and thermal conductivity, high mechanical resistance, low density, high visible light absorption and high transmission to the IR radiation [13, 14].

The prepared foils were characterized using different analysis techniques, such as X-ray photoelectron spectroscopy (XPS), SEM, Raman spectroscopy, characteristic X-ray fluorescence induced by electron beams (EDX), Rutherford backscattering spectroscopy (RBS) and elastic recoil detection analysis (ERDA) [15–17]. The composition of the pristine GO and of the thermal reduced GO and some properties are reported in table 1. The atomic ratio C/O increases in rGO, due to the reduction of functional oxygen groups chemically bonded to the GO during the reduction phase, the mass density ρ, the electrical conductivity σ and the thermal conductivity k increase significantly during the GO reduction phase, in agreement with the literature [16, 18, 19].

The rGO foils were covered with a thin metallic film of Al, Cu, Ag and Au, having 200 nm thickness. The physical vapor deposition technique was employed in a vacuum. The film thickness was measured accurately using 5.6 MeV alpha energy loss produced by ^{241}Am isotope source in the prepared covering film and the alpha stopping powers calculated by SRIM code.

The main ion detectors were SiC solid state Schottky barrier diodes, having up to 80 micron active regions when polarized inversely at 600 V. These detectors offer some advantages with respect to the traditional Si detectors exposed to plasma. Their higher gap energy of 3.3 eV blinds them to visible light, but not to UV and X-rays, their leakage current is of the order of 1 pA at room temperature, they can also operate at high temperature and their radiation damage occurs at high doses. Other SiC properties and construction aspects are given in the literature [20, 21]. SiCs are connected in time-of-flight (TOF) configuration in order to give the ion energy using the known flight distance and the recording of the spectra on a fast storage oscilloscope. Generally, the flight distance was fixed to 82 cm. The SiC detectors were placed at 0° and near a little angle ($\pm$3° and $\pm$10°) in forward direction using TNSA approach. Some filters in Al and mylar with thickness between 12 μm and 24 μm were placed in front of some detectors to separate fast protons from slowly ions.

An ion collector (IC) based on a Faraday cup with an electron suppression grid was employed in TOF approach.

A scheme of the used experimental set-up is reported in figure 2a.

The laser pulse shape vs. time is reported in figure 2b, indicating a contrast ASE of 10^{-8} and a pedestal duration of about 400 fs, while the main pulse duration is only 45 fs.
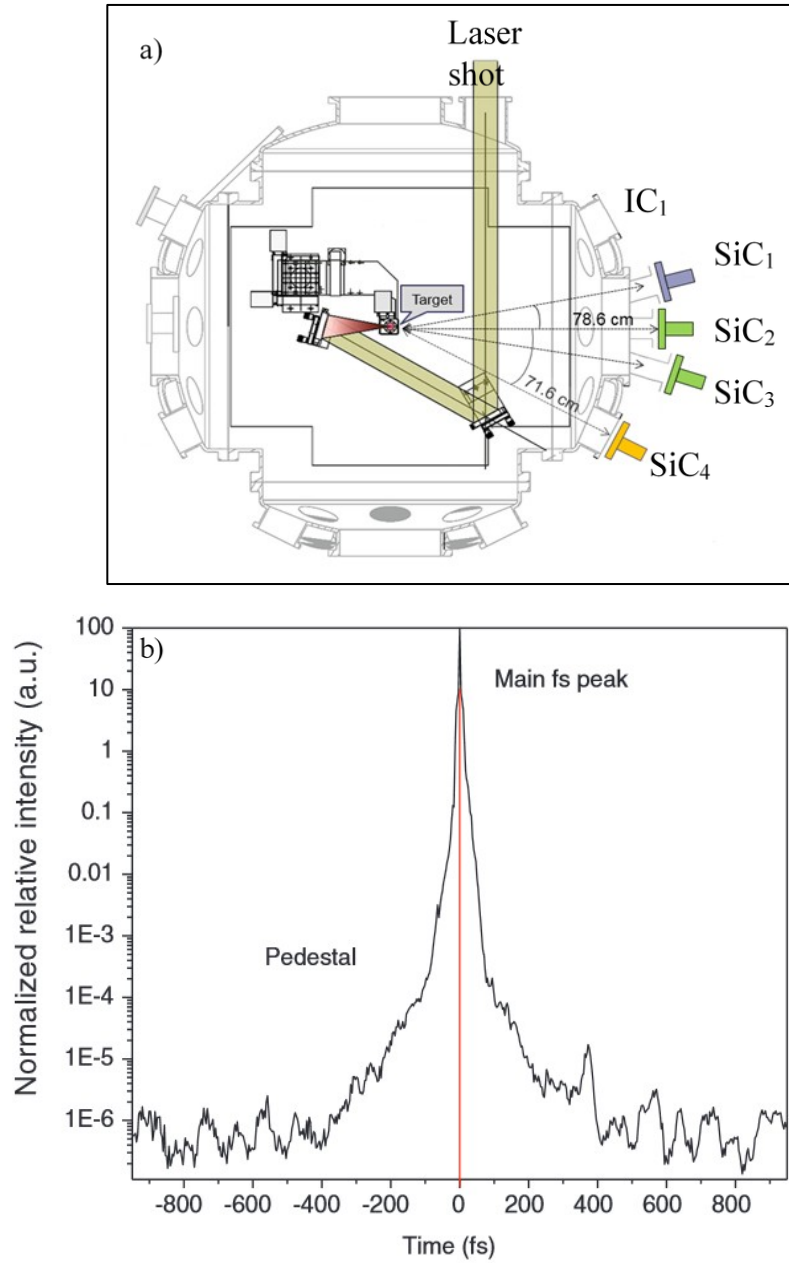
Figure 2. Scheme of the used experimental set-up (a) and laser pulse shape (b).

3 Results

Figure 3a reports a spectrum relative to the SiC TOF analysis of the 7 μm rGO irradiated in TNSA regime using a laser pulse energy of 290 mJ, an incidence angle of 0° and a laser focal position FP = 0 μm, i.e. focusing on the target surface. The spectrum shows a photopeak, due to the detection of X-rays and relativistic electrons, a detection of low energy electrons and a high and large peak due to the detection of ions. The faster ions are due to protons detection at a maximum energy of about 1 MeV.

The ion yield discontinuity observed at 80 ns and the very high ion yield due to the presence of ions accelerated by the rGO target indicate the presence of two ion species, i.e. the detection of protons and carbon ions.
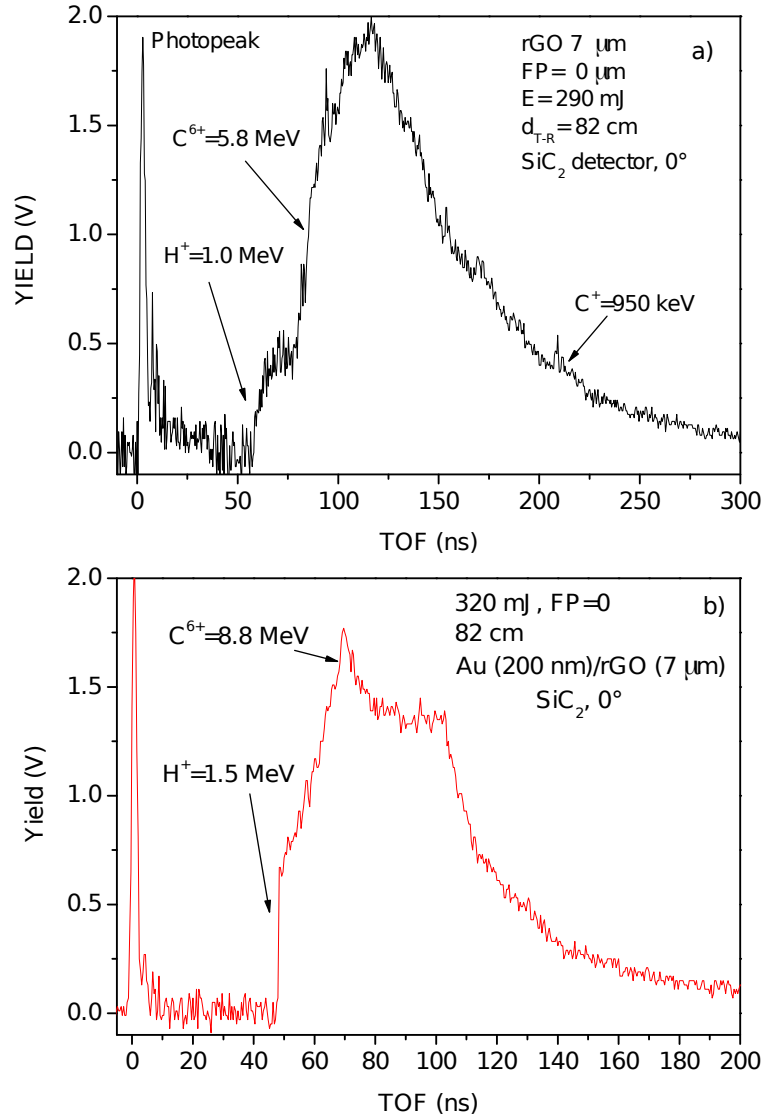

Figure 3. SiC TOF spectrum relative to the irradiation of 7 μm rGO (a) and 200 nm Au film covering the 7 μm rGO foil (b) using FP = 0 μm.

This aspect is confirmed by the literature relative to similar experimental results of proton and carbon ion acceleration by *fs* laser-generated plasma, which are in agreement with the theoretical results of particle-in-cell (PIC) simulations [22].

From the spectrum discontinuity separating the proton and the carbon ion contributions, at about 85 ns it is possible to derive the maximum kinetic energy of C ions corresponding to about 5.8 MeV. This energy is six times higher with that of faster protons, indicating that ions can be six times ionized, in agreement with the Coulomb-Boltzmann-Shifted (CBS) theory [23].

Thus, we assumed that plasma contains C^{6+} ions because they are submitted to the same electric field of the protons acceleration. At this stage, we have not used yet a Thomson parabola equipment. However, the yield tail of the ion peak, corresponding to the detection of slower C^{1+} ions that the TOF spectrum associates with an energy of about 0.95 MeV, confirms the carbon ion detection also.

This result indicates that the proton acceleration from rGO target increases with respect to that obtainable from graphite, carbon glassy, carbon in polymers and other type of carbon based materials. In fact, as presented in the literature, the use of similar laser intensities and experimental conditions, never allowed us to accelerate protons near to 1 MeV in energy [3, 7, 22]. This confirms that the advanced rGO target permits generating high proton acceleration thanks to its high surface electrical conductivity.

Figure 3b shows the SiC TOF spectrum relative to the TNSA irradiation of 200 nm Au film covering the 7 μm rGO foil with the same conditions of the previous spectrum (320 mJ, FP = 0 μm). In this case, the faster protons are characterized by a maximum kinetic energy of about 1.5 MeV, as result of the higher electron density of the non-equilibrium plasma induced by the Au coverage.

In addition, in this case the spectrum indicates the presence of C ions at different charge state from C^{6+} at about 9 MeV up to C^{1+} at about 1.5 MeV, indicating that such light ions are submitted to the same electric field driving the proton acceleration. No evidence of accelerated Au ions is detected also observing high TOF times.

The ion acceleration can be increased changing the focal position of the laser and choosing an area of the sample surface less wrinkled as possible with the online optical microscope. The optimal conditions were obtained using FP = +340 μm, i.e. focusing beyond the sample surface, increasing in this manner the spot areas on the gold surface.

Figure 4a reports the spectrum, relative to the results of protons acceleration maximization for the Au(200 nm)/rGO(7 μm) target. It was irradiated at 351 mJ, indicating a maximum proton energy of about 3.0 MeV and an ion yield compatible with the acceleration of C^{6+} ions at 18 MeV, of the other charge states of carbon ions up to C^{1+} at 3 MeV energy, also in this case in agreement with the CBS [23].

Figure 4b shows the results of proton acceleration maximization for the Ag(200 nm)/rGO(7 μm) target irradiated at 350 mJ with FP = +300 μm. The spectrum indicates a maximum proton energy of about 2.5 MeV and an ion yield compatible with the acceleration of C^{6+} ions at 15 MeV, of the other charge states of carbon ions up to C^{1+} at 2.5 MeV energy.

By irradiating the targets constituted by 200 nm Cu and Al deposited as thin film on the rGO, 7 μm thick, in the same experimental condition of the previous cases, the obtained TOF spectra are reported in figure 5a and 5b, respectively. The proton acceleration maximization was obtained using a focalization at FP = +200 μm for Cu target and +100 μm for Al target. The maximum proton kinetic energy was 2.1 MeV and 1.7 MeV for the Cu(200 nm)/rGO(7 μm) and Al(200 nm)/rGO(7 μm) targets, respectively.

Thus, from such results is evident that the proton acceleration enhances with the atomic number Z of the metallic film covering the rGO surface. This result is expected because the electrical field E driving the ion acceleration depends on the relation [24]:

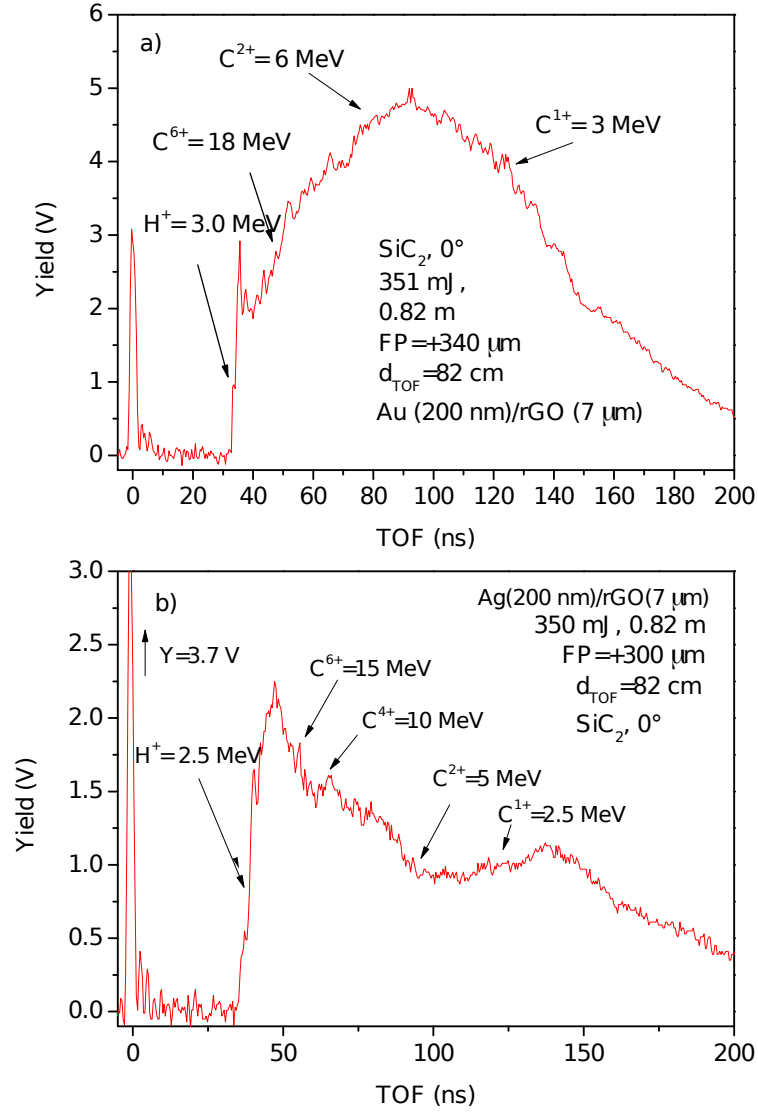$$E = \sqrt{\frac{2kTn_e}{\varepsilon_0}} \tag{3.1}$$

Figure 4. Spectrum relative to the protons acceleration optimization for the irradiation of Au(200 nm)/rGO(7 μm) target with FP = +340 mm (a) and Ag(200 nm)/rGO(7 μm) target with FP = +300 μm (b).

where kT and n_e are the electron temperature and the electron density of the plasma, and ε_0 is the vacuum permittivity. Thus increasing Z increases n_e and kT and consequently the electric field driving the ion acceleration.

Figure 6a reports the maximum proton acceleration, obtained optimizing the focal position conditions per each target, as a function of the atomic number of the metallic film covering the rGO foil. Results indicate a near linear trend with the atomic number of the covering metallic film.

The reported spectra from figure 4 to figure 5 indicate also other two information concerning the results obtained maximizing the proton acceleration, the first concerns the focal position FP, which increases with Z, and the second the photopeak yield, which results inversely proportional to Z, as presented in figure 6b.
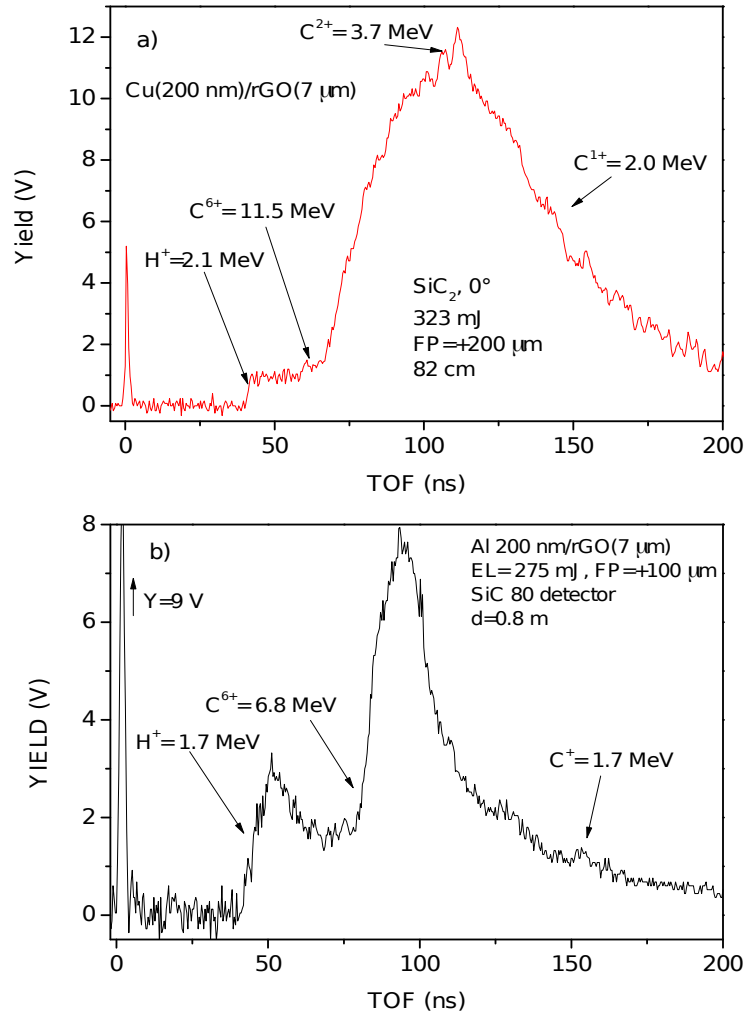
Figure 5. Spectrum relative to the proton acceleration optimization for the irradiation of 200 nm Cu/rGO (7 μm) (a) and of 200 nm Al/rGO (7 μm) (b).

The FP growth with Z indicates that, in order to maximize the proton acceleration, the laser spot on the foil surface must be enhanced. The spot increment, in fact, increases the number of relativistic electrons accelerated by the laser light, which are transmitted to the rear side of the target to drive the proton acceleration, and this phenomenon seems to be proportional approximately to the target surface electrical conductivity.

The photopeak decrement with the atomic number Z is not in disagree with measurements giving an increment of the X-ray peak production with Z [25]. Presented data, in fact, are obtained in different conditions of laser focal position FP, which decrease from Al up to Au. This means that the laser spot has a minimum value for Al (FP = +100 μm) and a major value for Cu (FP = +200 μm), Ag (FP = +300 μm) up to the Au (FP = +350 μm). Thus, for Al target a near minimum spot is used, the intensity is higher and the X-ray intensity also. For Au target, at which the optimal acceleration is for FP = +350 μm, at which the laser spot is larger, the laser intensity is minor and
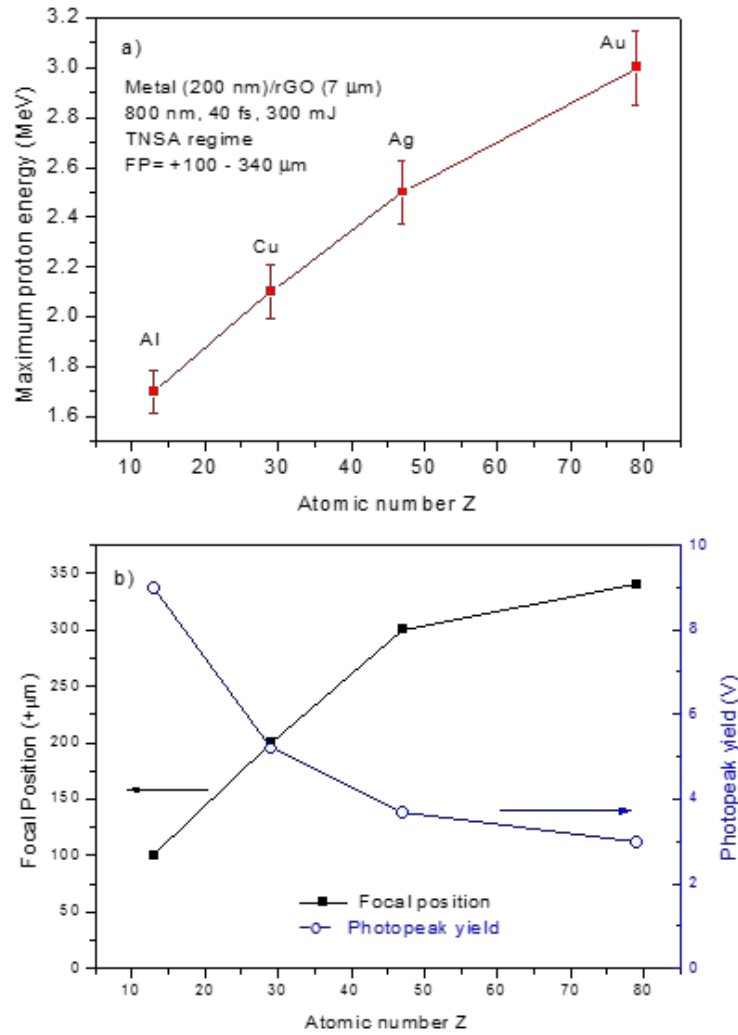
Figure 6. Maximum proton acceleration as a function of the atomic number Z of the used film (a) and optimization focal position vs. Z and corresponding photopeak yield vs. Z (b).

the X-ray intensity also. For this reason, changing the FP, i.e. the laser spot on the target, the laser intensity changes reducing with Z. Moreover, another reason of the photopeak reduction with Z, less important than the previous one, is due to the effect of laser reflection by the over critical density of the solid surface. The reflection, in fact, reduces the laser energy transferred to the plasma and it decreases going from Al, at which the reflectivity is $R = 0.87$, to Cu, Ag and up Au ($R = 0.99$) indicating that in the case of Au less energy is transferred to the plasma and less photon emission can be produced.

The photopeak is due to the contribution of X-rays and relativistic electrons detected by the SiC. Its yield decrement with the atomic number means that more laser energy is converted into X-rays for aluminum with respect to Au films, which, instead, permits converting more laser energy in proton and carbon ion energy. In fact, this observation is agreed with the total ion yield which is higher for Au films and lower for Al ones.

Thus, the different properties of the used metallic coverage films, some of which are reported in table 2, influence the final TNSA proton acceleration. For example, the surface reflectance may induce a partial laser pulse energy loss in overcritical surfaces, a contribution higher for Au with respect to Al films. The rGO at the used laser wavelength has a near negligible reflectivity [26].

Table 2. Some properties of the used metallic thin films and rGO foil.

Material	Al	Cu	Ag	Au	rGO
Z	13	29	47	79	12
σ $(\Omega\,cm)^{-1}$, 20°C	3.5×10^5	5.96×10^5	6.30×10^5	4.10×10^5	1.0
ρ (ats/cm^3)	6×10^{22}	8.5×10^{22}	5.8×10^{22}	5.9×10^{22}	7.5×10^{22}
Reflectivity (810 nm)	0.87	0.96	0.96	0.99	0.07

Although in this experiment no Thomson parable was used, the separation of fast protons, slow protons and carbon ions was possible thanks to the use of thin absorber films placed in front of the SiC detectors.

An example of ion recognition is presented in the spectra comparison reported in figure 7a relative to the analysis of the ions detected irradiating the Au/rGO target without absorber (higher red spectrum), with 12 µm mylar absorber (middle black spectrum) and with 23 µm mylar absorber (lower blue spectrum).

The 12 microns mylar permits to transmit only protons with energy higher than 700 keV and carbon ions with energy higher than 11 MeV.

Thus, the middle spectrum is relative to the detection of protons with energy between 2.85 MeV and 700 keV and carbon ions with energy between 17 MeV and 11 MeV, absorbing all the slowly ions. The 23 microns mylar permits to transmit only protons with energy higher than 1.1 MeV and carbon ions with energy higher than 20 MeV. Thus, the lower spectrum is relative to the detection of only protons with energy between 2.85 MeV and 1.1 MeV without carbon ion contribution. Thus, the differences between the middle spectrum and the lower is indicative of the contribution of more energetic carbon ions and of the more energetic protons, as indicated by the ion energy distributions deconvolved with a Boltzmann-like function.

A similar deconvolution for the faster protons and carbon ions is presented in figure 7b, relatively to the ion spectra comparison obtained irradiating the Ag/rGO target and detecting without filter (higher red spectrum), with 12 µm aluminum absorber (middle black spectrum) and with 24 µm aluminum absorber (lower blue spectrum).

The 12 microns Al permits to transmit only protons with energy higher than 900 keV and carbon ions with energy higher than 14 MeV. Thus, the middle spectrum is relative to the detection of protons with energy between 2.5 MeV and 0.9 MeV and carbon ions with energy between 15 MeV and 14 MeV, absorbing all the slowly ions. The 24 microns Al permits to transmit only protons with energy higher than 1.4 MeV and carbon ions with energy higher than 28 MeV. Thus, the lower spectrum is relative to the detection of only protons with energy between 2.5 MeV and 1.4 MeV without carbon ion contribution. Thus, the differences between the middle spectrum and the lower is indicative of the contribution of more energetic carbon ions and of the more energetic protons, as indicated by the ion energy distributions deconvolved with a Boltzmann-like function.
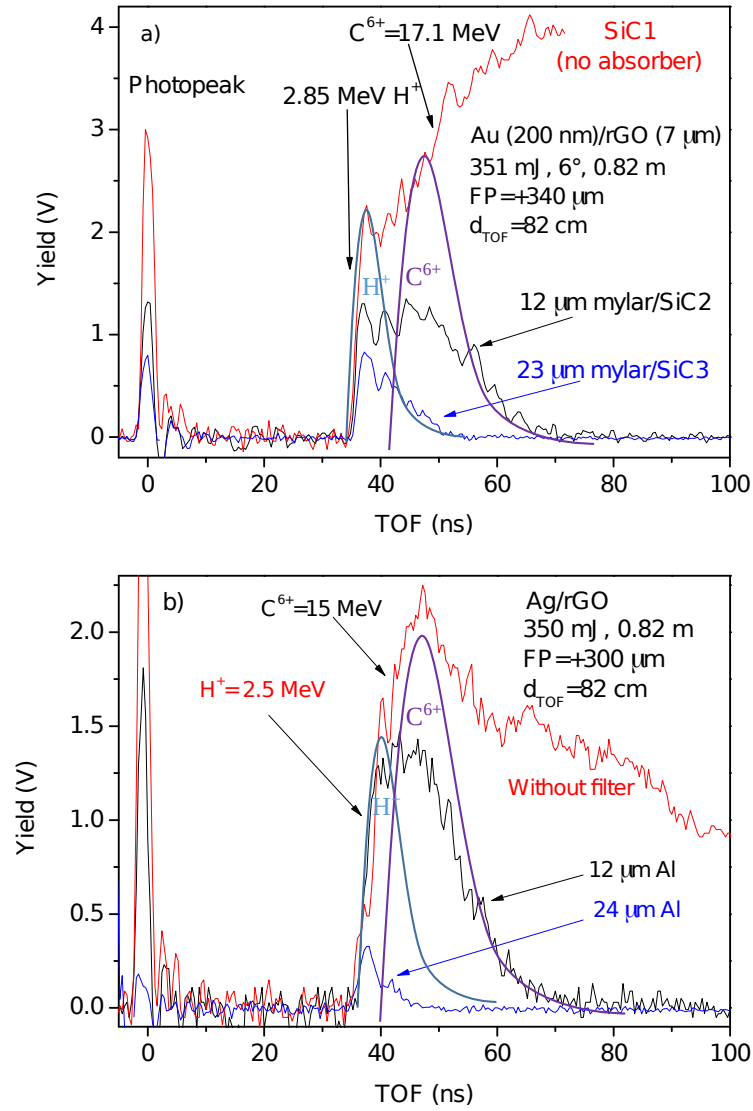
Figure 7. Spectra comparison for the irradiation of the Au(200 nm)/rGO and SiC detection without absorber and with 12 μm and 23 μm mylar absorber (a) and of the Ag(200 nm)/rGO and detection without absorber and with 12 μm and 24 μm Al absorber (b).

4 Discussion and conclusions

This paper reports about the possibility to accelerate protons and carbon ions using the TNSA regime and fs lasers at intensities of 10^{19} W/cm^2. The laser is employed with a focal spot size of 9 microns in diameter, a high contrast of 10^{-8} and a normal incidence angle ($\sim 0°$).

Advanced targets based on reduced graphene oxide, with micrometric platelets parallel to the film surface were employed with a thickness of 7 μm. Such targets, with respect to graphite permit to enhance the forward proton acceleration reaching about 1 MeV. The surface coverage of the rGO foil with a thin metallic film, 200 nm in thickness, enhances the proton acceleration reaching 3 MeV when the Au coverage film is employed. The acceleration improvement is attributed to the

higher electron density n_e of the plasma produced by this high conductive and high Z element. The plasma temperature kT instead is correlated to the deposited energy surface density, i.e. to the laser spot size on the target surface. Employing Au films kT can be maintained high also using relatively larger laser spot on the target which permits to accelerate a high number of relativistic electrons when the laser focusing position is inside the target with FP = +340 μm, i.e. the laser spot size on the target is high, of about 18 μm in diameter. Using Al film Z is lower and to maintain high kT the spot size must be reduced, for example using FP = +100 μm, at which its spot is 12 μm in diameter. Experimental data demonstrated that the maximum proton acceleration energy E_p depends on the empirical equation:

$$E_p = 10 \cdot \frac{Z}{\pi r^2} \quad (\text{MeV}) \tag{4.1}$$

where r is the spot radius in microns. Thus, considering a spot radius of 9 μm for Au (FP = 340 μm), 8 μm for Ag (FP = 300 μm), 7 μm for Cu (FP = 200 μm), and 6 μm for Al (FP = 100 μm), the obtained maximum proton energy meets eq. (4.1).

Of course, the maximum proton energy can be further improved, for example, acting on three important parameters to be further investigated. The first is the thickness of the used rGO, which was fixed to 7 microns in this experiment, but, as reported in the literature [27], the optimal thickness should be found checking lower and higher thicknesses. The second is the thickness of the covering metal, which was fixed to 200 nm in this experiment, but that should be further investigated on the role of thicker and thinner covering films. The third is the level of reduction of the used rGO, which electrical and thermal conductivity, energy band, optical and mechanical properties can be modified acting on the thermal treatment of reduction, as reported in the literature [13, 14, 16, 28].

An interesting aspect of the paper concerns the use of thin absorber film, which demonstrate that the emitted ions can be selected in energy and mass. For example, the use of 24 micron Al absorber permits to transmit only the protons with energy between 3 MeV and 1.4 MeV avoiding the transmission of slow protons and carbon ions and making the beam almost monochromatic.

Acknowledgments

References

[1] J. Badziak, *Laser-driven ion acceleration: methods, challenges and prospects*, *J. Phys. Conf. Ser.* **959** (2018) 012001.

[2] L. Torrisi, M. Cutroneo, L. Andò and J. Ullschmied, *Thomson parabola spectrometry for gold laser-generated plasmas*, *Phys. Plasmas* **20** (2013) 023106.

[3] L. Torrisi, M. Cutroneo, M. Rosinski, J. Badziak, P. Parys, J. Wołowski et al., *Near-3-MeV protons from target-normal-sheath-acceleration femtosecond laser irradiating advanced targets*, *Contrib. Plasma Phys.* **59** (2019) e201800127.

[4] M. Blanco, M.T. Flores-Arias, C. Ruiz and M. Vranic, *Table-top laser-based proton acceleration in nanostructured targets*, *New J. Phys.* **19** (2017) 033004.

[5] M. Borghesi, *Laser-driven ion acceleration: State of the art and emerging mechanisms*, *Nucl. Instrum. Meth.* **A 740** (2014) 6.

[6] M. Roth and M. Schollmeier, *Ion Acceleration-Target Normal Sheath Acceleration*, in *Proceedings of the CAS-CERN Accelerator School: Plasma Wake Acceleration*, B. Holzer ed., Geneva, Switzerland, 23–29 November 2014, pp. 231–270 [CERN-2016-001] [arXiv:1705.10569].

[7] L. Torrisi, M. Cutroneo, A. Torrisi, M. Rosinski, A. Zaras-Szydlowska and P. Parys, *Investigation of the effect of plasma waves excitation on target normal sheath ion acceleration using fs laser-irradiating hydrogenated structures*, *Contrib. Plasma Phys.* **59** (2019) e201900029.

[8] T. Nakamura, M. Tampo, R. Kodama, S.V. Bulanov and M. Kando, *Interaction of high contrast laser pulse with foam-attached target*, *Phys. Plasmas* **17** (2010) 113107.

[9] L. Torrisi, L. Calcagno, D. Giulietti, M. Cutroneo, M. Zimbone and J. Skala, *Laser irradiations of advanced targets promoting absorption resonance for ion acceleration in TNSA regime*, *Nucl. Instrum. Meth.* **B 355** (2015) 221.

[10] J. Badziak, S. Jabloński, T. Pisarczyk, T. Chodukowski, P. Parys, P. Rączka et al., *The LICPA accelerator of dense plasma and ion beams*, *J. Phys. Conf. Ser.* **508** (2014) 012006.

[11] Graphenea, *Graphene Oxide Water Dispersion*, https://www.graphenea.com/collections/graphene-oxide/products/graphene-oxide-4-mg-ml-water-dispersion-1000-ml.

[12] L. Torrisi, M. Cutroneo, V. Havranek, L. Silipigni, B. Fazio, M. Fazio et al., *Self-supporting graphene oxide films preparation and characterization methods*, *Vacuum* **160** (2019) 1.

[13] M. Aliofkhazraei, N. Ali, W.I. Milne, C.S. Ozkan, S. Mitura and J.L. Gervasoni, *Electrical and Optical Properties*, CRC Press, Taylor&Francis group, Boca Raton (2016).

[14] M. Aliofkhazraei, N. Ali, W.I. Milne, C.S. Ozkan, S. Mitura and J.L. Gervasoni, *Graphene Science Handbook — Mechanical and Chemical Properties*, CRC Press, Taylor&Francis group, Boca Raton (2016).

[15] M. Cutroneo, L. Torrisi, J. Badziak, M. Rosinski, V. Havranek, A. Mackova et al., *Graphite oxide based targets applied in laser matter interaction*, *EPJ Web Conf.* **167** (2018) 02004.

[16] L. Silipigni, G. Salvato, G. D. Marco, B. Fazio, A. Torrisi, M. Cutroneo et al., *Band-like transport in high vacuum thermal reduced graphene oxide films*, *Vacuum* **165** (2019) 254.

[17] L. Torrisi, L. Silipigni, V. Havranek, M. Cutroneo, A. Torrisi and G. Salvato, *Reduced graphene oxide foils for ion stripping applications*, *Radiat. Eff. Def. Solids* **174** (2019) 973.

[18] O.M. Slobodian, P.M. Lytvyn, A.S. Nikolenko, V.M. Naseka, O.Y. Khyzhun, A.V. Vasin et al., *Low-temperature reduction of graphene oxide: Electrical conductance and scanning kelvin probe force microscopy*, *Nanoscale Res. Lett.* **13** (2018) 139.

[19] Y. Zeng, T. Li, Y. Yao, T. Li, L. Hu and A. Marconnet, *Thermally conductive reduced graphene oxide thin films for extreme temperature sensors*, *Adv. Funct. Mat.* (2019) 1901388.

[20] M. Cutroneo, P. Musumeci, M. Zimbone, L. Torrisi, F. La Via, D. Margarone et al., *High performance SiC detectors for MeV ion beams generated by intense pulsed laser plasmas*, *J. Mat. Res.* **28** (2012) 87.

[21] A. Torrisi, P. Wachulak, L. Torrisi, A. Bartnik, Ł. Węgrzyński and H. Fiedorowicz, *Plasma characterization of the gas-puff target source dedicated for soft x-ray microscopy using SiC detectors*, *Nukleonika* **61** (2016) 139.

[22] L. Torrisi and G. Costa, *Ion acceleration by fs laser in target-normal-sheath-acceleration regime and comparison of time-of-flight spectra with particle-in-cell simulations*, *Phys. Rev. Accel. Beams* **23** (2020) 011304.

[23] L. Torrisi, *Coulomb-Boltzmann-shifted distribution in laser-generated plasmas from 10^{10} up to 10^{19} W/cm^2 intensities*, *Radiat. Eff. Def. Solids* **171** (2016) 34.

[24] L. Torrisi, M. Cutroneo, A. Torrisi, L. Silipigni, G. Costa, M. Rosinski et al., *Protons accelerated in the target normal sheath acceleration regime by a femtosecond laser*, *Phys. Rev. Accel. Beams* **22** (2019) 021302.

[25] L. Torrisi et al., *Laser-plasma X-ray detection by using fast 4H-SiC interdigit and ion collector detectors*, 2015 *JINST* **10** P07009.

[26] A. Nandi, S. Majumdar, S. K. Datta, H. Saha and S.M. Hossain, *Optical and electrical effects of thin reduced graphene oxide layers on textured wafer-based c-si solar cells for enhanced performance*, *J. Mater. Chem.* **C 5** (2017) 1920.

[27] L. Torrisi, *Laser contrast and other key parameters enhancing the laser conversion efficiency in ion acceleration regime*, *EPJ Web Conf.* **167** (2018) 02002.

[28] W. Park, J. Hu, L.A. Jauregui, X. Ruan and Y.P. Chen, *Electrical and thermal conductivities of reduced graphene oxide/polystyrene composites*, *Appl. Phys. Lett.* **104** (2014) 113101.